Journal of Magnetic Resonance **143,** 223–228 (2000)
doi:10.1006/jmre.1999.2003, available online at http://www.idealibrary.com on IDEAL®

Sensitivity Gain by Simultaneous Acquisition of Two Coherence Pathways: The HNCA$^+$ Experiment

Michael Salzmann,*,†,[1] Alfred Ross,*,[2] Michael Czisch,‡ and Gerhard Wider†

*F. Hoffmann–La Roche AG, Pharma Research, CH-4070 Basel, Switzerland; †Institute for Molecular Biology and Biophysics, Eidgenössische Technische Hochschule Hönggerberg, CH-8093 Zürich, Switzerland; and ‡Bijvoet Center for Biomolecular Research, University Utrecht, NL-3584 CH Utrecht, The Netherlands

Received August 18, 1999; revised November 15, 1999

In most multidimensional nuclear magnetic resonance experiments a single and distinct coherence transfer pathway is selected by phase cycling or by pulsed field gradients. It was shown that simultaneously exploiting more than one coherence transfer pathway could increase the overall sensitivity of NMR experiments. However, sensitivity enhancement schemes described to date introduce additional delays in the pulse schemes, resulting in considerable decrease of the expected sensitivity gain when applied to biomolecules due their fast transverse relaxation. A novel sensitivity enhancement principle which increases sensitivity of an experiment by simultaneously exploiting two completely independent coherence pathways in a single NMR pulse scheme is presented in this paper. As an example an improved HNCA experiment, the HNCA$^+$, is presented, which combines the "out-and-back" coherence transfer pathway used in HNCA with an "out-and-stay" experiment, analogous to HCANH, without adding any time periods compared to the conventional HNCA pulse sequence. The applicability of the HNCA$^+$ was theoretically evaluated with regard to different sizes of peptides or proteins, which showed that the experimental time can be reduced twofold in ideal cases. The application of this novel experiment to a 7-kDa protein showed a 20% sensitivity gain of HNCA$^+$ when compared to conventional HNCA.

Key Words: **coherence transfer; HCANH; (HA)CANH; HNCA; sensitivity gain.**

Multidimensional nuclear magnetic resonance (NMR) experiments are based on homo- and/or heteronuclear coherence transfers. Most sequences are characterized by a single, distinct coherence transfer pathway (CTP), selected by phase cycling or by pulsed field gradients (*1*). However, some NMR pulse sequences simultaneously monitor more than one pathway of coherence transfer in a single experiment. For example the homonuclear two-dimensional exclusive correlation experiment (E.COSY) (*2*) selects for double and triple quantum coherences. Proper weighting of the two CTPs results in a simplified spectrum when compared to a normal COSY spectrum (*3, 4*). Another example is the combined correlation/nuclear Overhauser experiment (COCONOESY) (*5*), where COSY and NOESY are recorded simultaneously. Further examples are the 2D HSMQC experiment (*6*), a combination between heteronuclear multiple-quantum coherence (HMQC) and heteronuclear single-quantum coherence (HSQC) experiments, and the recently developed heteronuclear 3D HXYH (*7*) and 3D HNHCACO pulse sequences (*8*). Not only spectral simplification or increased information content in a single spectrum but also the gain of sensitivity is a reason to exploit more than one CTP in a single experiment. Sensitivity enhancement techniques (*1, 9–12*) are applicable to many common NMR pulse sequences; however, these schemes may introduce additional delays, which may lead to a considerable decrease in sensitivity for large biomolecules due to fast transverse relaxation (T_2). The signal gain obtained from a sensitivity enhancement scheme introduced into a particular pulse sequence is therefore a compromise between additional relaxation losses and the theoretically obtainable enhancement factor.

Here we present a novel principle which increases sensitivity of an experiment by simultaneously exploiting two completely different coherence pathways in a single NMR pulse scheme. As an example we developed an improved HNCA experiment, refered to as the HNCA$^+$, which combines two different CTPs without adding any time periods compared to the conventional HNCA pulse sequence (*13, 14*). The HNCA$^+$ experiment combines a so-called "out-and-back" coherence transfer pathway, where the magnetization is detected on the same spin from which it originated, with an "out-and-stay" experiment, where the magnetization originates from a spin different from the one on which it is detected. Figure 1 shows the pulse sequence of the HNCA$^+$ experiment, in which both coherence transfer pathways contribute to the final signal. The first pathway corresponds to a HNCA experiment as described in the literature (*13*). The second contribution results from a pathway that starts with α-proton magnetization and ends as amide proton magnetization, analogous to a HCANH experiment (*15, 16*).

[1] Current address: BRUKER AG, Industriestrasse 26, CH-8117 Fällanden, Switzerland.

[2] To whom correspondence should be adressed. Fax: ++41-61-688 7408. E-mail: alfred.ross@roche.com.

1090-7807/00 $35.00

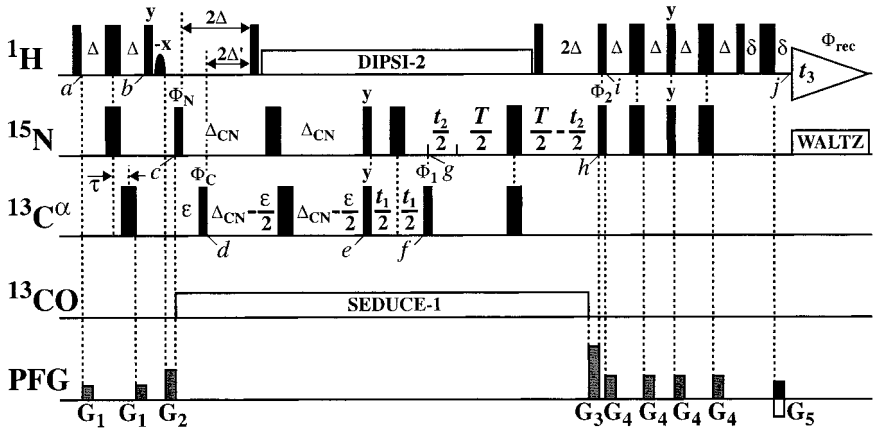

FIG. 1. Pulse sequence for the HNCA$^+$ experiment. Narrow and wide black bars represent 90° and 180° pulses, respectively. The black sinc profile at time point b denotes a selective water flip-back pulse of 1 ms length with a Gaussian shape truncated at 5%. Pulses for which the phases are not indicated are applied with phase x. The delays were set as follows: $\Delta = 2.7$ ms, $\tau = 1$ ms, $\epsilon = 1.8$ ms, $\Delta' = 1.7$ ms, $\Delta_{CN} = 13$ ms, and $T = 26$ ms. All gradient pulses have a sine shape and are applied along the z-axis. The duration and strengths of the gradients were set to 1 ms/6 Gcm^{-1} (G_1), 1 ms/30 Gcm^{-1} (G_2), 1.75 ms/14 Gcm^{-1} (G_3), 1 ms/7 Gcm^{-1} (G_4), and 177.3 μs/12 Gcm^{-1} (G_5), respectively. The phase cycle was $\Phi_1 = 2(y, -y, y, -y)$, $\Phi_2 = 2(x, x, -x, -x)$, $\Phi_N = \Phi_C = 4x, 4(-x)$, $\Phi_{rec} = (x, -x, -x, x, -x, x, x, -x)$. The phase Φ_1 is incremented according to the States-TPPI method (*22*). The phase Φ_2 is inverted together with the receiver phase and the sign of the gradient G_5 for each $^{15}N(t_2)$-increment and the data is processed according to Kay *et al.* (*11*). The phase Φ_C is inverted in a second experiment in order to seperate the pure ^{15}N-path and the pure ^{13}C-path spectrum during processing of the final spectrum. The combination of the two data sets is described in the text. Decoupling is achieved with the use of a SEDUCE-1 decoupling sequence (*23*) on carbonyl, DIPSI-2 decoupling sequence (*21*) on protons, and WALTZ-16 (*24*) on the ^{15}N channel during acquisition. The corresponding radio frequency field strengths were 0.83, 5, and 1.25 kHz, respectively.

Initial amide and α-proton polarization are transfered via two simultaneous INEPT transfers (*17*) to ^{15}N and ^{13}C, respectively, from where they evolve *via* different pathways. The final signal is obtained by properly processing the contributions from both pathways. Thus, the signal of the additional CTP is exploited to increase the sensitivity of the HNCA experiment, although the theoretical sensitivity gain by a factor of $\sqrt{2}$ is reduced by relaxation on the additional CTP. We show experimentally that this modification leads to a sensitivity gain of 20% for the small protein 434-repressor with 63 amino acids when compared to the common HNCA experiment (*14*).

In the following we describe both coherence transfer pathways exploited in the HNCA$^+$ experiment. For the sake of simplicity we only calculate the coherence transfers that contribute to the intraresidual signal. The calculation including the intraresidual and the preceding α-carbon can be done in full analogy. The normal out-and-back type contribution can be written in a short notation as

$$^1H^N \rightarrow {}^{15}N^H \rightarrow {}^{13}C^\alpha(t_1) \rightarrow {}^{15}N^H(t_2) \rightarrow {}^1H^N(t_3),$$

where $^1H^N$, $^{15}N^H$, and $^{13}C^\alpha$ stand for the polypeptide backbone amide proton, nitrogen, and α-carbon nuclei, respectively, and t_1, t_2, and t_3 indicate the chemical shift evolution times. This pathway, in the following refered to as the ^{15}N-path, is used in the conventional HNCA (*13*). The additional pathway in the HNCA$^+$, refered to as the ^{13}C-path, is of the out-and-stay type starting with the α-protons, which can be summarized as (*15, 16*)

$$^1H^\alpha \rightarrow {}^{13}C^\alpha(t_1) \rightarrow {}^{15}N^H(t_2) \rightarrow {}^1H^N(t_3),$$

where $^1H^\alpha$ stands for the polypeptide backbone α-proton. Note that the chemical shift evolution periods and the detection are on the same nuclei for both pathways. In general, the faster T_2 relaxation of the $^{13}C^\alpha$ nuclei will reduce the sensitivity of this path compared to the ^{15}N-path.

Using the product operator formalism (*18*) the two CTPs can be described as follows: Initial amide and α-proton magnetization $-H_y^N$ and $-H_y^\alpha$, respectively, obtained after the first 90° proton pulse (time point *a*) in Fig. 1 evolve into antiphase magnetization $2H_x^N N_z$ and $2H_x^\alpha C_z$ (time point b) (*19*). The 180° inversion pulse on carbons is shifted by $\tau = \Delta - \Delta'$ with respect to the 180° pulse on ^{15}N in order to account for the difference of $^1J(^1H^N, {}^{15}N^H)$ and $^1J(^1H^\alpha, {}^{13}C^\alpha)$ coupling constants (*17*). Completing the INEPT transfer the two antiphase terms $2H_z^N N_y$ and $2H_z^\alpha C_y$ are obtained at time points c and d, respectively. The water magnetization is flipped back to the positive z-axis by the selective pulse on the water resonance after time point b (*20*). The terms $2H_z^N N_y$ and $2H_z^\alpha C_y$ are refocused with respect to protons during the following delays 2Δ and $2\Delta'$ and then ^{1}H-decoupled with a DIPSI-2 sequence (*21*). Simultaneously the ^{15}N and ^{13}C magnetizations evolve into antiphase with respect to α-carbon and nitrogen during the delay $2\Delta_{CN}$, respectively. Thus, at time point e we obtain the terms $-2N_yC_z$ and $-2C_yN_z$. The subsequent carbon and nitrogen 90° pulses, both applied with phase $+y$, produce multiple-quantum coherences, which evolve due to the ^{13}C chemical shift during the t_1 evolution period. At the

end of t_1 (time point f) the following coherences of interest are present:

$$^{15}\text{N-path: } -2N_yC_x\cos(\omega_C t_1) - 2N_yC_y\sin(\omega_C t_1) \quad [1a]$$

$$^{13}\text{C-path: } -2C_yN_x\cos(\omega_C t_1) + 2C_xN_x\sin(\omega_C t_1). \quad [1b]$$

The following ^{13}C 90° pulse with phase Φ_1 (time point f) is used for the quadrature detection in the carbon dimension by applying a phase incrementation according to States-TPPI (*1*, *22*). This pulse creates the following coherences at the beginning of the constant-time ^{15}N-evolution period t_2 (time point g):

^{15}N-path:

$$\begin{aligned} &-2N_yC_x\cos(\omega_C t_1) \mp 2N_yC_z\sin(\omega_C t_1) \quad (\Phi_1 = \pm x)\\ &\pm 2N_yC_z\cos(\omega_C t_1) - 2N_yC_y\sin(\omega_C t_1) \quad (\Phi_1 = \pm y) \end{aligned} \quad [2a]$$

^{13}C-path:

$$\begin{aligned} &\mp 2C_zN_x\cos(\omega_C t_1) + 2C_xN_x\sin(\omega_C t_1) \quad (\Phi_1 = \pm x)\\ &-2C_yN_x\cos(\omega_C t_1) \mp 2C_zN_x\sin(\omega_C t_1) \quad (\Phi_1 = \pm y). \end{aligned} \quad [2b]$$

Since the multiple-quantum terms in Eq. [2] will not contribute to the detected signal they will be omitted for the rest of the calculation. The relevant antiphase terms in Eq. [2] evolve due to the ^{15}N chemical shift during the constant-time evolution period t_2 and refocus due to the $^1J(^{15}N^H, {}^{13}C^\alpha)$ coupling during T. After the ^{1}H-decoupling is switched off the magnetization evolves into antiphase with respect to the amide protons due to the $^1J(^1H^N, {}^{15}N^H)$ coupling during the period 2Δ.

The following sensitivity enhancement scheme between the time points i and j retains both the real and the imaginary part of the ^{15}N magnetization produced during the t_2 evolution period as described by Kay *et al.* (*11*). Thus, at time point j prior to acquisition the following magnetization components are present for the different settings of the phase Φ_1 and $\Phi_2 = +x$, respectively:

^{15}N-path:

$$\begin{aligned} &\pm(H_y\cos(\omega_N t_2)\sin(\omega_C t_1) + H_x\sin(\omega_N t_2)\sin(\omega_C t_1))\\ &\quad (\Phi_1 = \pm x)\\ &\mp(H_y\cos(\omega_N t_2)\cos(\omega_C t_1) + H_x\sin(\omega_N t_2)\cos(\omega_C t_1))\\ &\quad (\Phi_1 = \pm y) \end{aligned} \quad [3a]$$

^{13}C-path:

$$\begin{aligned} &\pm(H_y\sin(\omega_N t_2)\cos(\omega_C t_1) - H_x\cos(\omega_N t_2)\cos(\omega_C t_1))\\ &\quad (\Phi_1 = \pm x)\\ &\pm(H_y\sin(\omega_N t_2)\sin(\omega_C t_1) - H_x\cos(\omega_N t_2)\sin(\omega_C t_1))\\ &\quad (\Phi_1 = \pm y). \end{aligned} \quad [3b]$$

For all combinations of the Φ_1 and Φ_2 phases, which enable the quadrature detection in the two indirect dimensions, two signal contributions are obtained: the signal described by Eq. [3a], which corresponds to that of a regular HNCA experiment, and the additional signal in Eq. [3b], which leads to the observed gain in sensitivity.

As is seen from Eq. [3], the signal contributions from the different pathways are phase-shifted by 90° with respect to both indirect dimensions for a given pair of phases Φ_1/Φ_2. As the cosine-modulation yields the real and the sine-modulation the imaginary part in the indirect dimensions, these phase-shifts can be interpreted as a reversed recording of the real and the imaginary parts of the ^{15}N- and the ^{13}C-paths, respectively. For example, if the ^{15}N-path yields a purely cosine-modulated signal $\cos(\omega_N t_2)\cos(\omega_C t_1)$, the ^{13}C-path simultaneously contributes a purely sine-modulated signal for the same phase settings Φ_1/Φ_2. Pure absorption mode lineshape is achieved by incrementing the phase Φ_C of the 90° pulse on ^{13}C (time point d) by 180° in a second experiment—a technique used in other sensitivity enhancement schemes (*1*, *9–12*). This sign-reversal on the ^{13}C-path will propagate throughout the whole sequence, whereas coherences evolving on the ^{15}N-path are not affected. In this second experiment the observable proton magnetization originating from the ^{13}C-path will be of opposite sign as that given in Eq. [3b]. Addition of the first and the second experiment for a particular Φ_1 and Φ_2 setting thus yields the pure ^{15}N-path HNCA data set, whereas subtraction of the two experiments yields the pure ^{13}C-path (HA)CANH data set. After Fourier transformation the latter has to be phase-shifted by 90° in both indirect dimensions and can then be summed to the ^{15}N-path spectrum.

In the following we want to focus on some technical details of the HNCA$^+$ pulse sequence. The 90° pulse on ^{13}C at time point d (Fig. 1) is applied approximately 2 ms after that on ^{15}N at time point c, which initiates evolution into antiphase magnetization $-2N_yC_z$ on the ^{15}N-path. Thus, the 90° pulse on ^{13}C (time point d) may disturb this evolution by flipping the carbon nuclei. Figure 2a shows the simulated transfer functions for the ^{15}N- and the ^{13}C-paths as a function of the delay ϵ between the time points c and d. Optimal sensitivity is obtained with $\epsilon = 1.8$ ms. The loss of magnetization on the ^{15}N-path due to the carbon pulse is only 1% (Fig. 2a).

Since the ^{13}C-path uses α-carbon magnetization, which is in the transverse plane during the period $2\Delta_{CN} - \epsilon$, fast carbon T_2 relaxation constitutes a potential limitation to the HNCA$^+$ experiment. However, it should be noted that even if the ^{13}C-path would not contribute any signal, the final data can be processed to achieve a spectrum identical to that of a normal HNCA. The curves in Fig. 2b show the transfer functions of the ^{13}C- and the ^{15}N-paths versus the delay $2\Delta_{CN}$ between time points c and e, respectively, using a delay $\epsilon = 1.8$ ms. The coherence on the ^{15}N-path is modulated by a cosine function due to the coupling to both the intramolecular and the sequential α-carbons, whereas the transfer function for the ^{13}C-path shows a more complicated behavior due to the additional $^1J(^{13}C^\alpha, {}^{13}C^\beta)$ coupling constant. For a typical period $2\Delta_{CN}$ of 26 ms and a protein with a rotational correlation time τ_c of 5 ns

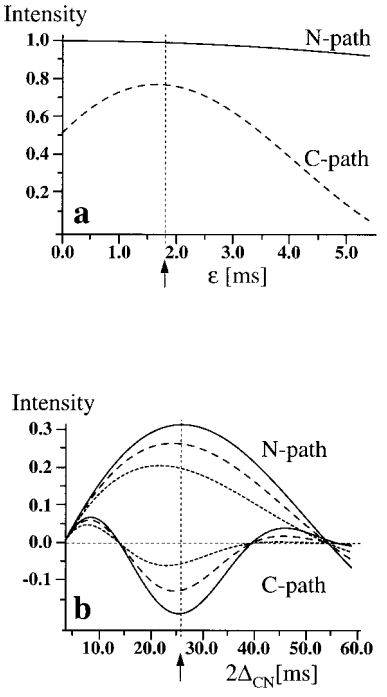

FIG. 2. (a) Intensity of the magnetization transfered via the ^{15}N- and ^{13}C-paths in dependence of the delay ϵ before the 90° pulse on ^{13}C is applied at time point d in Fig. 1. The maximum intensity on the ^{13}C-path (broken line) is obtained for $\epsilon = 1.8$ ms as indicated by the arrow, where the disturbance of the evolution into $-2N_yC_z$ coherence on the ^{15}N-path (solid line) is negligible (a). The effect of transverse relaxation has been neglected for simulating the curves. (b) Plot of the signal intensity versus the length of the delay $2\Delta_{CN}$ (Fig. 1) for different transverse relaxation times. The curves show the signal intensity resulting from the ^{15}N-path (top three curves), which is equal to the conventional HNCA signal, and the ^{13}C-path (bottom three lines), respectively, using $\epsilon = 1.8$ ms. For a typical value of $2\Delta_{CN} = 26$ ms (arrow), the additional signal from the ^{13}C-path is about 60% of that of a small protein with a correlation time τ_c of 5 ns (solid line). For a protein with $\tau_c = 10$ ns the contribution is 40% (dashed line), and for a protein with $\tau_c = 20$ ns the sensitivity is approxiamtely 20% (dotted line). The curves have been calculated using the coherence transfer functions for the corresponding CTPs in the HNCA$^+$ experiment, which were multiplied by an exponential function reflecting transverse relaxation. The corresponding relaxation rates were calculated for the different correlation times assuming dipolar coupling with the directly attached proton as the only source for relaxation. The ^{15}N and $^{13}C^{\alpha}$ T_2 relaxation times thus were 192 and 52 ms for $\tau_c = 5$ ns, 96 and 26 ms for $\tau_c = 10$ ns, and 48 and 13 ms for $\tau_c = 20$ ns, respectively.

(solid line in Fig. 2b), the signal of the ^{13}C-path in the HNCA$^+$ is about 60% of that in the ^{15}N path data set. For a medium-size protein with $\tau_c = 10$ ns the contribution from the ^{13}C-path is about 40% (dashed line), and for larger proteins with $\tau_c = 20$ ns the signal contribution from the ^{13}C-path in the HNCA$^+$ is expected to be 20% when compared to the conventional HNCA (dotted line).

We recorded both the HNCA (*14*) and the HNCA$^+$ experiment with the 63 amino acid protein 434-repressor. The first (^{1}H, ^{15}N)-plane of the conventional HNCA spectra is shown in Fig. 3: Both the real (Fig. 3A) and the imaginary parts (Fig. 3B) of the first ^{13}C time increment, $t_1 = 0$, are shown. The real part is recorded with $\Phi_1 = +y$ selecting for a cosine-modulation $\cos(\omega_C t_1)$ with respect to the ^{13}C evolution and the imaginary part with $\Phi_1 = +x$, selecting for a sine-modulation $\sin(\omega_C t_1)$. For $t_1 = 0$ only $\cos(\omega_C t_1)$ terms contribute signals whereas the imaginary part is zero (Fig. 3B). For comparison, the same (^{1}H,^{15}N)-planes recorded with the HNCA$^+$ pulse sequence are shown in Figs. 3C and 3D, respectively. Since the

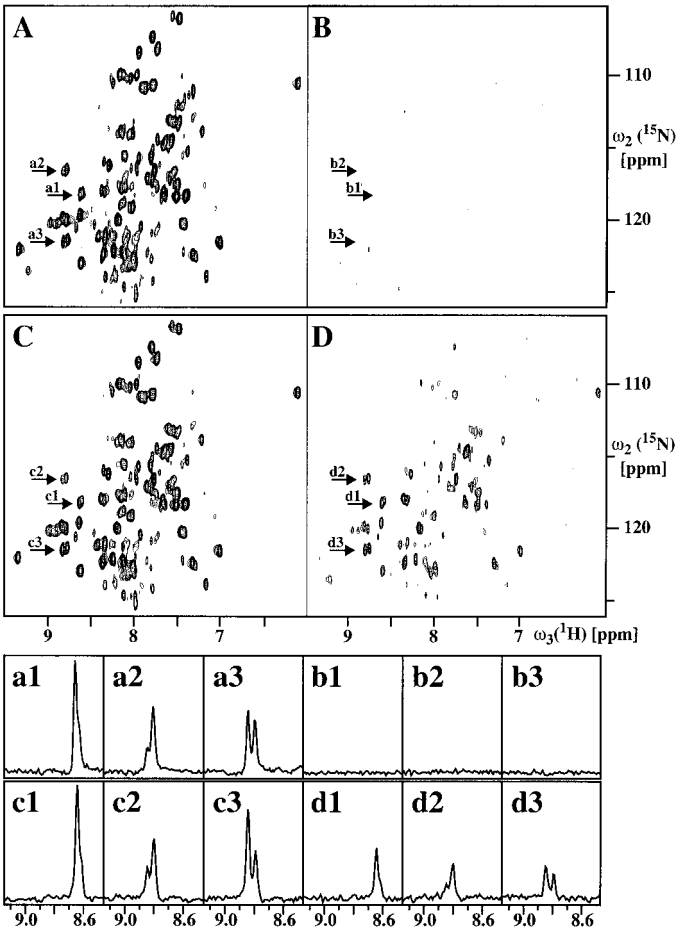

FIG. 3. Spectra of ^{13}C,^{13}N-labeled 434-repressor recorded on a Bruker DRX 600-MHz spectrometer. The sample concentration was 1 mM at pH 7.0 and the spectra were recorded at 298 K. The first (^{1}H,^{15}N) planes of two 3D HNCA experiments with the ^{13}C evolution time $t_1 = 0$ are shown. Both the real (A, C) and the imaginary parts (B, D) with respect to the ^{13}C dimension are shown. (A, B) Recorded with the conventional gradient-enhanced HNCA experiment (*14*); (C, D) recorded with the new HNCA$^+$ scheme. The real parts (A and C) contain the same signal with the same intensity for all resonances. The imaginary part of the first (^{1}H,^{15}N) plane is zero for the conventional HNCA (B), whereas a signal is recorded in case of the HNCA$^+$ (D). By adding up the real and imaginary parts in both experiments as described in the text. (a–d) Cross-sections parallel to the ω_3 axis taken from the corresponding 2D spectra A–D at a ω_2 chemical shift indicated by the arrows in the contour plots. The cross-sections a and c from the real parts (A, C) contain the same signal intensity, whereas only the imaginary part of the HNCA$^+$ (D) yields additional signal (d). ^{1}H and ^{15}N sweep widths of 9616 and 4464 Hz were acquired with 128 scans per t_2 increment. The spectral resolution was 1024 × 44 complex points.

signal is described by Eq. [3a] in both cases the real part (Fig. 3C) contains exactly the same signal as shown in Fig. 3A. But, in contrast to the regular HNCA experiment, the imaginary part (Fig. 3D) contains signal as well. This signal results from the cosine-modulated terms with respect to the carbon dimension of the ^{13}C-path (Eq. [3b]). Noteworthy, the signals from the Gly-residues are missing in this spectrum, since they are in antiphase at the beginning of the ^{1}H-decoupling period due to their evolution under the coupling to the two attached α-protons. Cross-sections along the $\omega_3(^{1}\mathrm{H})$-dimension of the 2D spectra in Figs. 3A to 3D, taken at a ^{15}N chemical shift indicated by the corresponding arrows, are shown in the corresponding Figs. 3a–3d. The signal intensities in Figs. 3a and 3c are the same; the additional signal resulting from the ^{13}C-path in the HNCA^{+} experiment is shown in Fig. 3d.

The summation of the signal obtained from the ^{15}N-path, S_N, and the ^{13}C-path, S_C, to the resulting signal, S_r, must be properly done to achieve optimal signal-to-noise ratio S_r/N_r for the combined spectrum. In general the ^{13}C-path data has to be added to the one of the ^{15}N-path with an optimized weighting factor λ:

$$\frac{S_r}{N_r} = \frac{S_N + \lambda S_C}{\sqrt{N_N^2 + \lambda^2 N_C^2}} = \frac{S_N + \lambda S_C}{\sqrt{1 + \lambda^2} \cdot N_N}, \qquad [4]$$

where N_r is the noise in the final spectrum and N_N and N_C the noise in the ^{15}N-path spectrum and the ^{13}C-path spectrum, respectively. Due to the 90° phase correction applied to the ^{13}C-path spectrum with respect to the ^{15}N-path spectrum the N_N and N_C noise are independent, however, obviously with the same noise power $N_N^2 = N_C^2$. Equation [4] can analytically be solved for the largest ratio S_r/N_r, which results in

$$\lambda = \frac{S_C/N_C}{S_N/N_N}, \qquad [5]$$

i.e., the spectrum of the ^{13}C-path has to be weighted with the ratio of the signal-to-noise ratios of the ^{13}C-path and ^{15}N-path spectra. The value of λ depends particularly on the T_2 of the $^{13}\mathrm{C}^{\alpha}$ resonances: If the individual relaxation rates differ significantly, λ should be adjusted separately for the different groups of resonances. For the 434-repressor the resulting HNCA^{+} spectrum has on average 40% increased sensitivity compared to the conventional HNCA using $\lambda = 0.6$. As can be seen from Eq. 3 this sensitivity gain obtained from recording the ^{13}C-path not only holds for the first but also for all increments of the $^{13}\mathrm{C}(t_1)$-evolution.

We have shown that by a simple modification of the HNCA experiment, the recording of an additional coherence transfer pathway becomes possible, which can result in a significant gain in sensitivity. The additional coherence transfer pathway in the novel HNCA^{+} experiment uses the simultaneous transfer of α-proton magnetization to $^{13}\mathrm{C}^{\alpha}$ in addition to the normal transfer from the amide proton to the attached $^{15}\mathrm{N}^{\mathrm{H}}$. The comparison of the HNCA^{+} and the HNCA experiment shows that up to twofold reduction in experimental time can be achieved depending on the size and mobility of the protein under investigation. The technique should preferably be used for smaller proteins and peptides with a molecular weight of up to 15 kDa.

REFERENCES

1. G. Wider, Technical aspects of NMR spectroscopy with biological macromolecules and studies of hydration in solution, *Prog. Magn. Reson. Spectr.* **32,** 193–275 (1998).
2. C. Griesinger, O. W. Sørensen, and R. R. Ernst, Correlation of connected transitions by two-dimensional NMR spectroscopy, *J. Chem. Phys.* **85,** 6837–6852 (1986).
3. W. P. Aue, E. Bartholdi, and R. R. Ernst, Two-dimensional spectroscopy. Application to nuclear magnetic resonance, *J. Chem. Phys.* **64,** 2229–2246 (1976).
4. J. Jeener, "Pulse pair techniques in high resolution NMR," Ampère International Summer School, Basko Polje, Yugoslavia (1971).
5. A. Z. Gurevich, I. L. Barsukov, A. S. Arseniev, and V. F. Bystrov, Combined COSY-NOESY experiment, *J. Magn. Reson.* **56,** 471–478 (1984).
6. E. R. P. Zuiderweg, A proton-detected heteronuclear chemical-shift correlation experiment with improved resolution and sensitivity, *J. Magn. Reson.* **86,** 346–357 (1990).
7. M. Mariani, M. Tessari, R. Boelens, H. Vis, and R. Kaptein, Assignment of the protein backbone from a single 3D, ^{15}N ^{13}C, time-shared HXYH experiment, *J. Magn. Reson. B* **104,** 294–297 (1994).
8. Y. Pang, L. Zeng, A. V. Kurochkin, and E. R. P. Zuiderweg, High-resolution detection of five frequencies in a single 3D spectrum: HNHCACO—A bidirectional coherence transfer experiment, *J. Biomol. NMR* **11,** 185–190 (1998).
9. A. G. Palmer III, J. Cavanagh, P. E. Wright, and M. Rance, Sensitivity improvement in proton-detected two-dimensional heteronuclear correlation NMR spectroscopy, *J. Magn. Reson.* **93,** 151–170 (1991).
10. A. G. Palmer III, J. Cavanagh, A. R. Byrd, and M. Rance, Sensitivity improvement in three-dimensional heteronuclear correlation NMR spectroscopy, *J. Magn. Reson.* **96,** 416–424 (1992).
11. L. E. Kay, P. Keifer, and T. Saarinen, Pure absorption gradient enhanced heteronuclear single quantum correlation spectroscopy with improved sensitivity, *J. Am. Chem. Soc.* **114,** 10663–10665 (1992).
12. S. S. Wijmenga, C. P. M. van Mierlo, and E. Steensma, Doubly sensitivity-enhanced 3D TOCSY-HSQC, *J. Biomol. NMR* **8,** 319–330 (1996).
13. S. Grzesiek and A. Bax, Improved 3D triple-resonance NMR techniques applied to a 31-kDa protein, *J. Magn. Reson.* **96,** 432–440 (1992).
14. D. R. Muhandiram and L. E. Kay, Gradient-enhanced triple-resonance three-dimensional NMR experiments with improved sensitivity, *J. Magn. Reson. B* **103,** 203–216 (1994).
15. G. T. Montelione and G. Wagner, Conformation-independent sequential NMR connections in isotope-enriched polypeptides by ^{1}H–^{13}C–^{15}N triple resonance experiments, *J. Magn. Reson.* **87,** 183–188 (1990).
16. L. E. Kay, M. Ikura, and A. Bax, The design and optimization of

complex NMR experiments. Application to a triple-resonance pulse scheme correlating H^{α}, NH, and ^{15}N chemical shifts in ^{13}C–^{15}N-labeled proteins, *J. Magn. Reson.* **91,** 84–92 (1991).

17. R. Boelens, M. Burgering, R. H. Fogh, and R. Kaptein, Time-saving methods for heteronuclear multidimensional NMR of (^{13}C, ^{15}N) doubly labeled proteins, *J. Biomol. NMR* **4,** 201–213 (1994).
18. O. W. Sørensen, G. W. Eich, M. H. Levitt, G. Bodenhausen, and R. R. Ernst, Product operator formalism for the description of NMR pulse experiments, *Prog. Magn. Reson. Spectr.* **16,** 163–192 (1983).
19. G. Bodenhausen and R. Freeman, Correlation of proton and carbon-13 NMR spectra by heteronuclear two-dimensional spectroscopy, *J. Magn. Reson.* **28,** 471–476 (1977).
20. S. Grzesiek and A. Bax, The importance of not saturating H_2O in protein NMR. Application to sensitivity enhancement and NOE measurements, *J. Am. Chem. Soc.* **115,** 12593–12594 (1993).
21. J. Cavanagh and M. Rance, Suppression of cross-relaxation effects in TOCSY spectra via a modified DIPSI-2 mixing sequence, *J. Magn. Reson.* **96,** 670–678 (1992).
22. D. Marion, M. Ikura, R. Tschudin and A. Bax, Rapid recording of 2D NMR spectra without phase cycling. Application to the study of hydrogen exchange in proteins, *J. Magn. Reson.* **85,** 393–399 (1989).
23. M. A. McCoy and L. Mueller, Selective shaped pulse decoupling in NMR: Homonuclear [^{13}C]carbonyl decoupling, *J. Am. Chem. Soc.* **114,** 2108–2112 (1992).
24. A. J. Shaka, J. Keeler, and R. Freeman, Evaluation of a new broadband decoupling sequence: WALTZ-16, *J. Magn. Reson.* **53,** 313–340 (1983).